Available online at www.sciencedirect.com
ScienceDirect
Journal of Catalysis 245 (2007) 144–155
JOURNAL OF CATALYSIS
www.elsevier.com/locate/jcat

Surface modification of Ni catalysts with trace Pt for oxidative steam reforming of methane

Baitao Li [a], Shigeru Kado [b], Yuya Mukainakano [b], Tomohisa Miyazawa [b], Toshihiro Miyao [c], Shuichi Naito [c], Kazu Okumura [d], Kimio Kunimori [b], Keiichi Tomishige [b,*]

[a] *College of Chemistry, South China University of Technology, Guangzhou 510640, China*
[b] *Institute of Materials Science, University of Tsukuba, 1-1-1 Tennodai, Tsukuba, Ibaraki 305-8573, Japan*
[c] *Department of Applied Chemistry, Faculty of Engineering, Kanagawa University, 3-27-1, Rokkakubashi, Kanagawa-ku, Yokohama, Kanagawa 221-8686, Japan*
[d] *Department of Materials Science, Faculty of Engineering, Tottori University, Koyama-cho Minami, Tottori 680-8552, Japan*

Received 5 April 2006; revised 25 September 2006; accepted 4 October 2006

Available online 1 November 2006

Abstract

Hysteresis of catalytic performance with respect to temperature increasing and decreasing in oxidative steam reforming of methane ($CH_4/H_2O/O_2/Ar = 40/30/20/10$) over the monometallic Ni catalysts disappeared by the modification with Pt, and the additive effect of Pt by the sequential impregnation method (Pt/Ni) was much more significant than that by the co-impregnation method (Pt + Ni) in terms of catalytic performance and catalyst bed temperature profile. Characterization results by means of TEM, TPR, EXAFS, and FTIR suggest that the Pt atoms on the Pt/Ni catalysts were located more preferably on the surface to form a Pt–Ni alloy than those on the Pt + Ni catalysts. The modification of Ni with Pt suppressed the oxidation of Ni species near the bed inlet in the oxidative steam reforming of methane at 1123 K, although the species on the monometallic Ni catalysts were oxidized under similar conditions. This can be due to the decreased oxidation rate of the species and the increased reduction rate caused by the surface modification of Ni with Pt. Consequently, the Pt–Ni species can be maintained in the metallic state near the bed inlet, and the species can be the active site for the reforming reaction as well as the combustion reaction, which this leads to a lower bed temperature and smaller temperature gradient than those seen for the monometallic Ni catalysts.

Keywords: Oxidative reforming; Steam reforming; Methane; Combustion; Pt; Ni; Thermography; Hot spot; Surface segregation

1. Introduction

Production of a synthesis gas using natural gas reforming is very important in the gas to liquid process [1,2]. A conventional and industrial method for syngas production is steam reforming of methane [2–4]. Steam reforming of methane is a highly endothermic reaction, as described below; therefore, external heating using methane combustion is required:

$$CH_4 + H_2O \rightarrow CO + 3H_2 \quad \Delta H^0_{298\ K} = +206\ \mathrm{kJ\,mol^{-1}}. \quad (1)$$

On the other hand, internal heat supplies are well known to be more energy efficient than external heat supply systems. A well-known internal heat supplying system for syngas production is the autothermal reforming process (ATR), which was developed by Haldor Topsoe [5]. In the ATR process, oxygen is fed together with methane and steam. The added oxygen engenders exothermic reactions, such as noncatalytic partial oxidation [Eq. (2)] and combustion of methane [Eq. (3)] in the noncatalytic reaction zone; this heat is used for the catalytic reforming reaction on the catalysts,

$$CH_4 + (1/2)O_2 \rightarrow CO + 2H_2 \quad \Delta H^0_{298\ K} = -36\ \mathrm{kJ\,mol^{-1}} \quad (2)$$

and

$$CH_4 + 2O_2 \rightarrow CO_2 + 2H_2O \quad \Delta H^0_{298\ K} = -803\ \mathrm{kJ\,mol^{-1}}. \quad (3)$$

In the ATR process, the contact between the reforming catalysts and oxygen is inhibited for suppression of hot-spot formation [6]. Hot-spot formation is a common problem in the

* Corresponding author. Fax: +81 29 853 5030.
E-mail address: tomi@tulip.sannet.ne.jp (K. Tomishige).

0021-9517/$ – see front matter © 2006 Published by Elsevier Inc.
doi:10.1016/j.jcat.2006.10.004

reforming of hydrocarbons to synthesis gas using oxygen [7,8]. The active component of conventional steam-reforming catalysts is Ni; however, in the presence of oxygen, Ni species can be oxidized and thereby lose their reforming activity [9–11]. On the other hand, after oxygen is consumed in the catalyst bed, Ni species can maintain their metallic state and contribute to the reforming reaction. As a result, a large temperature gradient appears because the exothermic and the endothermic reaction zones are separated completely [12–14]. The large temperature gradient over the catalyst bed can also be related to the hot-spot formation in catalytic partial oxidation of methane [15–18]. Recently, catalysts for oxidative steam reforming have been developed in connection with hydrogen production for fuel cells [19–21] and syngas production [22–24]. Our group has found that the temperature gradient of Pt and Rh was much smaller than that of Ni catalyst in oxidative steam reforming of methane [25,26]. This behavior is related to the lower oxygen affinity of Rh and Pt compared with that of Ni [27]; the small temperature gradient in the catalyst bed is explainable by the overlap of the combustion reaction zone with the reforming reaction zone. On the other hand, although Pd has low oxygen affinity, it has a larger temperature gradient than Ni catalyst because of the very low reforming activity of Pd catalysts [26]. Considering the high cost and limited availability of Pt and Rh, a decreased loading amount is desired. However, obtaining high activity of the catalysts with a very small loading quantity is difficult [28]. Our possible strategy of catalyst development for oxidative reforming of methane with high resistance to hot-spot formation is to use Pt–Ni bimetallic catalysts containing small amounts of Pt, in which the high reducibility of Pt and high reforming activity of Ni are applied. In addition, intermetallic compounds and alloys have been known to form between Pt and Ni [29–34]. Their strong interaction can be expected. Furthermore, the preparation method can influence the structure of the bimetallic particles and catalytic performance.

In this study, the Ni catalysts were modified with Pt in two methods (sequential impregnation [Pt/Ni] and co-impregnation [Pt + Ni]), and the modification effect of Pt was evaluated by catalytic performance and catalyst bed temperature profile in the oxidative steam reforming of methane. We found that the introduction of Pt to Ni catalysts by the sequential impregnation enhanced the catalytic performance and gave a flat bed temperature profile. The monometallic Pt and Ni catalysts and Pt–Ni bimetallic catalysts were characterized by temperature-programmed reduction (TPR), transmission electron microscopy (TEM), extended X-ray absorption fine structure (EXAFS), and Fourier transform infrared spectroscopy (FTIR). It is suggested that the modified Pt atoms are located more preferably on the surface of metal particles on the Pt/Ni catalysts prepared by the sequential impregnation method, and that these Pt atoms can contribute to the enhanced catalyst reducibility and keep Ni species metallic under the presence of oxygen. It is thought that this species can be the active site for the steam reforming of methane as well as methane combustion even under the presence of oxygen, which can explain the flat bed temperature profile and the suppression of hot-spot formation.

2. Experimental

2.1. Catalyst preparation

A commercially available γ-Al_2O_3 (JRC-ALO-1) (Catalysis Society of Japan, $S_{BET} = 143\ m^2\,g^{-1}$, grain size of 2–3 mm) was calcined at 1123 K in air for 3 h; it was used as a support material. The support thus obtained had a specific surface area of 110 $m^2\,g^{-1}$. It was crushed and sieved to particle sizes of 180–250 μm before impregnation. Supported monometallic Ni and Pt catalysts were prepared by wet impregnation using $Ni(NO_3)_2{\cdot}6H_2O$ (99.9%, Wako Pure Chemical Industries Ltd.) or $H_2PtCl_6{\cdot}6H_2O$ (99.9%, Soekawa Chemical Co., Ltd.). The catalyst was prepared by impregnating the support material with an aqueous solution of the precursor. After removal of the solvent by heating and evaporation at 353 K, the resulting product was dried in an oven at 383 K for 12 h. Subsequently, the sample was calcined at 773 K in air for 3 h. Bimetallic Pt–Ni catalysts were prepared by two methods: sequential impregnation and co-impregnation. In the sequential (two-step) impregnation method, the monometallic Ni catalysts mentioned above were used. Before the second impregnation, the calcined monometallic Ni catalysts were reduced with H_2 at 1123 K for 0.5 h. Then the Pt was loaded by impregnating the Ni catalysts with the acetone solution of $Pt(C_5H_7O_2)_2{\cdot}H_2O$ (99.9%; Soekawa Chemical Co., Ltd.) under air. After the acetone solvent was removed, the catalyst was dried at 383 K for 12 h and calcined in air at 573 K for 3 h. The resultant catalyst is denoted as Pt/Ni. In the co-impregnation method, the precursor was a mixture of aqueous solution of $Ni(NO_3)_2{\cdot}6H_2O$ and $H_2PtCl_6{\cdot}6H_2O$. After co-impregnation, the preparation procedure was identical to that of monometallic catalyst. This resultant catalyst is denoted as Pt + Ni. The number in parentheses refers to the weight percent of the catalyst's metallic component.

2.2. Activity test and thermographical observation

Oxidative steam reforming of methane was conducted under atmospheric pressure in a fixed-bed quartz reactor (i.d. 4 mm ∅, o.d. 6 mm ∅). The quartz reactor had an axial thermowell (o.d. 1.5 mm ∅) containing a chromel–alumel thermocouple located at the outlet of the catalyst bed, which was used for temperature control. The temperature indicated by the thermocouple is denoted as T_{TC}. An electronic furnace was connected with this thermocontroller; it had a window (15 mm × 15 mm) for observing the temperature profile of catalyst granules. The temperature profile was measured using infrared thermograph equipment (TH31; NEC San-ei Instruments Ltd.). The details of thermographical observation were described previously [28]. The catalyst (0.08 g) was reduced in the hydrogen flow (30 ml min^{-1}, 100% H_2) at 1123 K for 0.5 h in the reactor. After reduction, the feed gases (the mixture of CH_4, O_2, steam, and Ar) were introduced to the catalyst bed at various contact times W/F [W (g) = catalyst weight, F (mol h^{-1}) = total flow rate of gases]. Gases such as CH_4 (99.99%), O_2 (99.999%), H_2 (99.999%), and Ar (99.999%) were obtained from Takachiho

Trading Co. Ltd. The gases were used without further purification. Steam was obtained by vaporizing distilled water that was supplied using a feeding pump. The partial pressure ratio of the feeding gases was $CH_4/H_2O/O_2/Ar = 40/30/20/10$. An iced water trap was located at the reactor exit to remove the steam contained in the effluent gas. A part of the effluent gas was collected with a microsyringe through the septum equipped in the gas line. Then it was analyzed using a gas chromatograph (GC-14A; Shimadzu Corp.) equipped with a flame ionization detector (FID) and a thermal conductivity detector (TCD). Concentrations of CO, CO_2, and CH_4 in the effluent gas were determined using an FID-GC equipped with a methanator, with a stainless steel column packed with Gaskuropack 54 (GL Science). The H_2 concentration was determined using TCD-GC with a stainless steel column packed with a 13X molecular sieve. Methane conversion and CO selectivity in oxidative steam reforming of methane were calculated as

$$\text{methane conversion } (\%) = \frac{C_{CO} + C_{CO_2}}{C_{CH_4} + C_{CO} + C_{CO_2}} \times 100$$

and

$$\text{CO selectivity } (\%) = \frac{C_{CO}}{C_{CO} + C_{CO_2}} \times 100,$$

where C is the concentration of each gas in the effluent gas.

We also checked the amount of deposited carbon on the catalyst after the reaction; the amount was negligible in all results shown here. We also evaluated the catalytic performance and the bed temperature profiles of the catalysts with smaller granule size (140–180 μm) than used here. The behavior in the oxidative reforming of methane agreed well with the catalysts with the present granule size (180–250 μm). This indicates that the mass transport is not limited under the present experimental conditions. The catalytic performance in steam reforming of methane was also evaluated; the method and procedure were the same as in oxidative steam reforming of methane, except $T_{TC} = 1023$ K and the partial pressure ratio ($CH_4/H_2O/Ar = 30/30/40$).

2.3. Catalyst characterization

TPR profiles were measured in a fixed-bed quartz reactor. Each time, 0.01 g of sample was loaded into the quartz reactor and heated at a rate of 10 K min^{-1} from room temperature to 1273 K in 5% hydrogen diluted in argon (30 ml min^{-1}) as a reducing gas. Water produced during the reduction was removed using a cold trap with frozen acetone (ca. 173 K). The TPR profile was monitored continuously with an on-line TCD-GC to measure the partial pressure change of H_2 due to the consumption. The H_2 consumption was estimated from the integrated peak area of the reduction profiles.

Transmission electron microscope (TEM) images were obtained using a JEOL JEM-2010F microscope operated at 200 kV. First, the catalysts were reduced by H_2 pretreatment at 1123 K for 0.5 h in a fixed-bed reactor. Samples were dispersed in 2-propanol using supersonic waves. They were put on Cu grids for TEM observation under air atmosphere.

The Ni K-edge and Pt L_3-edge EXAFS were measured at the BL-9C station of the Photon Factory at the High-Energy Accelerator Research Organization in Tsukuba, Japan. The storage ring was operated at 2.5 GeV with a ring current of 300–450 mA. A Si(111) single crystal was used to obtain a monochromatic X-ray beam. The monochromator was detuned to 60% maximum intensity to avoid higher harmonics in the X-ray beam. Two ion chambers filled with N_2 and 25% Ar diluted with N_2 for Ni K-edge EXAFS were used to detect I_0 and I. In the case of Pt L_3-edge EXAFS, 15% Ar diluted with N_2 and Ar were used. The samples for the EXAFS measurement were prepared by pressing catalyst powders of 70 and 260 mg, respectively, for Ni K-edge and Pt L_3-edge EXAFS. The respective sample thicknesses were chosen as 0.5 and 1.9 mm, to give edge jumps of 0.20 and 0.06 for Ni K-edge and Pt L_3-edge EXAFS. The catalyst was treated by H_2 at 1123 K for 0.5 h in a fixed-bed reactor, and the samples were pressed into self-supporting 10-mm-diameter wafers. Then each sample was treated again with H_2 at 773 K for 0.5 h in the cell. After this pretreatment, each sample was transferred to the measurement cell using a glove box filled with nitrogen to prevent exposure of the sample disk to air. Passivated samples were prepared as follows. After the catalyst powder was reduced with H_2 at 1123 K, it was passivated with 0.5% O_2 in He in the fixed-bed reactor at room temperature. After the passivated catalysts were pressed into wafers, they were transferred to the measurement cell using a glove box filled with nitrogen, thereby preventing further exposure of the disk to air. EXAFS data were collected in a transmission mode at 77 K. For EXAFS analyses, the oscillation was first extracted from EXAFS data using a spline smoothing method [35]. The oscillation was normalized by the edge height around 50 eV. The Fourier transformation of the k^3-weighted EXAFS oscillation from k space to r space was performed to obtain a radial distribution function. The inversely Fourier filtered data were analyzed using a common curve-fitting method [36,37]. The Fourier transform and Fourier filtering ranges are given for each result. For the curve-fitting analysis, the empirical phase shift and amplitude functions for the Pt–Pt and Ni–Ni bonds were extracted from data for Pt and Ni foils. Theoretical functions for the Pt–Ni bond were calculated using the FEFF8.2 program [38]. Analyses of EXAFS data were performed using the "REX2000" program (Version: 2.3.3; Rigaku Corp.).

FTIR spectra were recorded using a spectrometer (Magna 550; Nicolet Biomedical Inc.) equipped with an MCT detector in transmission mode (resolution 4 cm^{-1}). An in situ IR quartz cell with CaF_2 windows was used. All samples for the IR measurement were treated in H_2 at 1123 K for 0.5 h in a fixed-bed reactor, as was done for the activity tests. After this treatment, the samples were pressed into self-supporting 20-mm-diameter wafers; each disk was about 150 mg. The sample disk was transferred to the IR cell connected to the closed circulation vacuum system, which was used to expose the sample to the adsorption and treatment gases. Then the sample was reduced with H_2 at 773 K for 0.5 h under 13 kPa. After the sample was cooled to room temperature during H_2 circulation, the environment was evacuated at room temperature. For CO adsorption, CO (0.13 kPa) was exposed to the sample at room

temperature; the spectra were obtained after evacuation at room temperature. The coverage of CO on each sample was almost complete at this CO pressure.

3. Results and discussion

3.1. Catalytic performance and bed temperature in the oxidative steam reforming of methane

Fig. 1 shows the dependence of methane conversion, CO selectivity, and H_2/CO ratio in oxidative steam reforming of methane as a function of T_{TC}. In the activity test, after the catalyst was reduced in H_2 flow at 1123 K for 0.5 h, T_{TC} was first decreased from 1123 to 773 K, then increased from 773 to 1123 K. The catalytic performance at each T_{TC} was observed for 15 min. In the profile of decreasing T_{TC} over monometallic Ni catalyst (Fig. 1a), methane conversion decreased drastically at $T_{TC} = 923$ K, due to the oxidation of active Ni species, as discussed later. It dropped to about zero when T_{TC} was below 873 K, where Ni catalyst lost its methane reforming and combustion activity. In contrast, in the profile of increasing T_{TC}, the catalytic activity of Ni(0.9) was not recovered until 1023 K. When T_{TC} was beyond 1023 K, methane conversion increased gradually; however, it did not reach the same conversion level as in the profile of decreasing T_{TC}.

An important finding on the Ni(0.9) catalyst is that methane conversion showed severe hysteresis with respect to decreasing and increasing T_{TC}. In contrast, hysteresis was not observed for the monometallic Pt(0.2), bimetallic Pt(0.2) + Ni(0.9), and Pt(0.2)/Ni(0.9) catalysts (Figs. 1b–1d); the behaviors in the profiles of increasing and decreasing temperature were almost identical. Regarding these three catalysts, the order of methane conversion was Pt(0.2) < Pt(0.2) + Ni(0.9) < Pt(0.2)/Ni(0.9) in the entire T_{TC} range. In addition, the sudden drop in methane conversion at $T_{TC} = 923$ K over the Ni(0.9) was not observed on Pt(0.2) + Ni(0.9) and Pt(0.2)/Ni(0.9). Although the details are not shown here, the tendencies of Pt(0.1), Ni(2.6), and corresponding bimetallic catalysts were similar, indicating that the addition of Pt also effectively promoted resistance to the oxidation of Ni even under much lower Pt-to-Ni ratios. Over the catalyst Pt(0.1)/Ni(2.6), the molar ratio of Pt/Ni was 0.01, much lower than the 0.06 on Pt(0.2)/Ni(0.9). The results indicate that the modification of Ni with Pt was effective for the oxidative steam reforming of methane and that the preparation method of the bimetallic catalyst influenced its catalytic performance, and that the sequential impregnation was more favorable. The low activity over Ni(0.9) at $T_{TC} \leqslant 923$ K may be due to the oxidation of Ni metal species, because the active species for the reforming reaction is known to be metallic Ni. Similar phenomena were observed in previous studies [21,39,40]. In addition, the W/F was chosen to be 0.16 g h mol^{-1}; the reforming re-

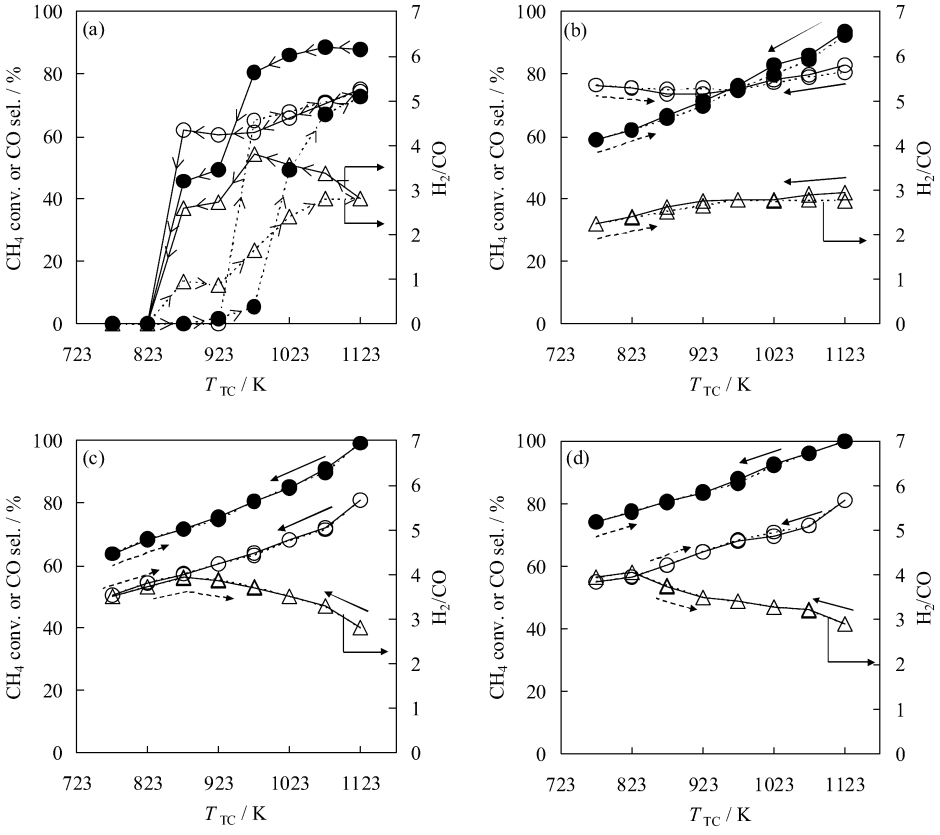

Fig. 1. Dependence of methane conversion, CO selectivity and H_2/CO ratio in oxidative steam reforming of methane as a function of T_{TC} over (a) Ni(0.9), (b) Pt(0.2), (c) Pt(0.2) + Ni(0.9), (d) Pt(0.2)/Ni(0.9). (●) Methane conversion, (○) CO selectivity, (△) H_2/CO, (—) decreasing temperature, (- - -) increasing temperature. Reaction conditions: $CH_4/H_2O/O_2/Ar = 40/30/20/10$; $W/F = 0.16$ g h mol^{-1}; total pressure 0.1 MPa; catalyst weight 0.08 g; H_2 pretreatment at 1123 K.

action did not reach the equilibrium in the T_{TC} range of 923–1123 K. The equilibrium states in terms of methane conversion and CO selectivity at 1123 K are listed in Table 1; those at 923 K were 85 and 62%, respectively. In addition, the equilibrium methane conversion at 773 K was 47%, lower than the experimental data over the catalysts except for Ni(0.9) at $T_{TC} = 773$ K. At $T_{TC} = 773$ K, the experimental methane conversion level was lower than 75% even when the O_2 conversion reached almost 100%. Considering the heat balance between the reforming and combustion reactions, the catalyst bed temperature can be higher than T_{TC}. The obtained conversion was apparently beyond the equilibrium at T_{TC}, however, this can be due to the temperature difference between T_{TC} and the catalyst bed at a reaction temperature below 923 K. Note that this kind of complicated behavior was not observed at reaction temperatures above 923 K under high methane conversion conditions.

Fig. 2 shows results of the thermographical observation during oxidative steam reforming of methane at $W/F = 0.16$ and 0.07 g h mol^{-1} over Pt(0.2)/Ni(0.9), Pt(0.2) + Ni(0.9), and their reference catalysts at $T_{TC} = 1123$ K. Table 1 lists the methane conversions, H_2/CO ratios, and CO selectivities. Two bimetallic catalysts showed slightly higher methane conversion than the monometallic Ni and Pt catalysts did; however, the difference in the catalyst bed temperature profiles was great. Fig. 2a shows the exothermic profile near the bed inlet over Ni(0.9) at $W/F = 0.16$ g h mol^{-1}, whereas for the three catalysts, flatter temperature profiles were observed. On the other hand, the exothermic profile of Ni(0.9) became more pronounced at $W/F = 0.07$ g h mol^{-1}, as shown in Fig. 2b. Two bimetallic catalysts and monometallic Pt(0.2) also showed exothermic profiles near the catalyst bed inlet. The order of the bed temperature was Ni(0.9) ≫ Pt(0.2) > Pt(0.2) + Ni(0.9) > Pt(0.2)/Ni(0.9). In addition, based on the results given in Table 1, it is possible to calculate the temperature of catalyst bed outlet assuming that the water–gas shift reaction reaches the reaction equilibrium. In all cases, the calculated temperatures are in the range of 1100–1150 K. When experimental errors for the gas analysis and the thermographical observation are considered, it appears that the obtained temperature agrees with the calculated one.

Table 1
Catalytic performance over Ni(0.9), Pt(0.2) and their corresponding bimetallic catalysts prepared by different methods in oxidative steam reforming of methane[a]

Catalyst	W/F (g h mol^{-1})	CH_4 conversion (%)	CO selectivity (%)	H_2/CO
Pt(0.2)/Ni (0.9)	0.07	>99	81	2.8
	0.16	>99	81	2.9
Pt(0.2) + Ni(0.9)	0.07	>99	80	2.8
	0.16	>99	81	2.8
Ni(0.9)	0.07	95	79	2.8
	0.16	88	75	2.8
Pt(0.2)	0.07	90	81	2.8
	0.16	92	81	2.8
Equilibrium	–	>99	81	2.9

[a] Reaction conditions: $CH_4/H_2O/O_2/Ar = 40/30/20/10$; $T_{TC} = 1123$ K; total pressure 0.1 MPa; catalyst weight 0.08 g; H_2 pretreatment 1123 K.

According to previous reports [25,26], the Pt catalysts exhibited flatter bed temperature profiles than the Ni catalysts. Here, in particular, the Pt(0.2)/Ni(0.9) gave a lower bed temperature profile than monometallic Pt(0.2) and Ni(0.9) catalysts. This result indicates that the synergistic effect of Pt and Ni in suppressing the increase in bed temperature in the oxidative steam reforming of methane. This synergistic effect was also clearly seen for catalysts with a lower molar ratio of Pt/Ni like Pt(0.1)/Ni(2.6) [28]. In addition, Pt(0.2)/Ni(0.9) and Pt(0.1)/Ni(2.6) catalysts were stable in terms of the bed temperature profile as well as methane conversion, CO selectivity, and H_2/CO at $T_{TC} = 1123$ K for 8 h. Furthermore, Table 2 compares steam reforming of methane and oxidative steam reforming of methane over Pt(0.1)/Ni(2.6), Pt(0.1) + Ni(2.6), and their reference catalysts. As listed in Table 2, the order of the catalytic activity in the steam reforming of methane was Ni(2.6) ≈ Pt(0.1) + Ni(2.6) > Pt(0.1)/Ni(2.6) > Pt(0.1), very different from that in the oxidative steam reforming of methane: Pt(0.1)/Ni(2.6) ≈ Pt(0.1) + Ni(2.6) > Ni(2.6) > Pt(0.1). It is intriguing that Pt(0.1)/Ni(2.6) showed higher activity in the oxidative steam reforming reaction, although its activity in the steam reforming without oxygen was lower. Unlike in the ox-

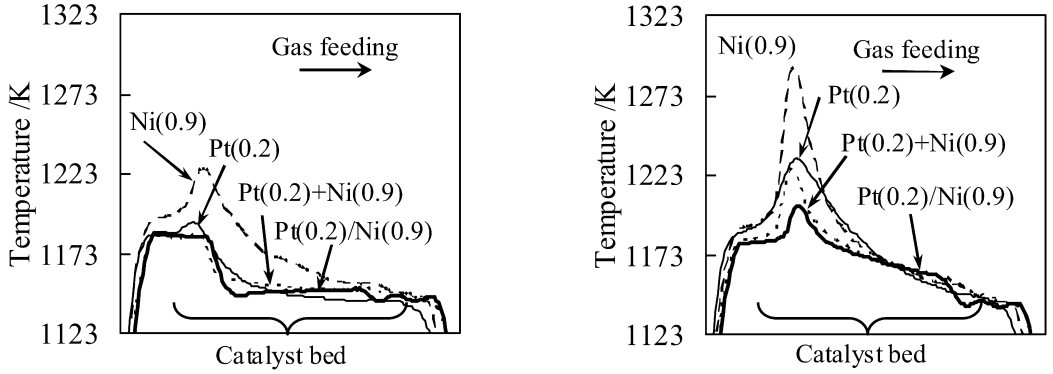

Fig. 2. Catalyst bed temperature profile in oxidative steam reforming of methane over various catalysts at $W/F = 0.16$ (a) and 0.07 g h mol^{-1} (b). Reaction conditions: $CH_4/H_2O/O_2/Ar = 40/30/20/10$; $T_{TC} = 1123$ K; total pressure 0.1 MPa; catalyst weight 0.08 g; H_2 pretreatment 1123 K.

idative steam reforming of methane, in the steam reforming of methane, the whole catalyst in the bed can be maintained in a reduced state because of the absence of O_2. This result suggests that the presence of oxygen leads to decreased reforming activity in Ni(2.6) and Pt(0.1) + Ni(2.6), due mainly to the oxidation of Ni, whereas Pt(0.1)/Ni(2.6) exhibited a high resistance to oxidation and maintained the activity even under the presence of oxygen. The detailed evaluation was done by TPR characterization over the samples after the oxidative steam reforming of methane reaction.

Table 2
Catalytic performance over Ni(2.6), Pt(0.1) and their corresponding bimetallic catalysts in steam reforming of methane and oxidative steam reforming of methane[a]

Reaction	Catalyst	CH_4 conversion (%)	CO selectivity (%)	H_2/CO
Steam reforming	Pt(0.1)/Ni(2.6)	41	68	4.9
	Pt(0.1) + Ni(2.6)	55	80	4.0
	Ni(2.6)	58	82	3.9
	Pt(0.1)	32	60	5.7
	Equilibrium	87	96	3.2
Oxidative steam reforming	Pt(0.1)/Ni(2.6)	>99	82	2.7
	Pt(0.1) + Ni(2.6)	>99	81	2.7
	Ni(2.6)	97	79	2.9
	Pt(0.1)	90	75	2.8
	Equilibrium	>99	81	2.9

[a] Reaction conditions: $CH_4/H_2O/O_2/Ar = 30/30/0/40$, $T_{TC} = 1023$ K for steam reforming; $CH_4/H_2O/O_2/Ar = 40/30/20/10$, $T_{TC} = 1123$ K for oxidative steam reforming; total pressure 0.1 MPa; catalyst weight 0.08 g; H_2 pretreatment 1123 K, $W/F = 0.16$ g h mol^{-1}.

3.2. Catalyst characterization

Fig. 3 presents TPR profiles of various catalysts to evaluate catalyst reducibility. Figs. 3a and 3e show the TPR profiles of the calcined Ni(0.9) and Ni(2.6) catalysts. The ratio of hydrogen consumption based on Ni content was almost 100%, and the consumption of H_2 was observed in the temperature range of 700–1160 K. This H_2 consumption peak is assigned to the reduction of highly dispersed NiO, which interacts strongly with the Al_2O_3 surface [41]. On the other hand, for Pt(0.2) + Ni(0.9) (Fig. 3b), the main reduction peak started at about 120 K lower than for Ni(0.9), suggesting that the addition of Pt promoted NiO reduction, as has been noted previously [40,42,43]. A similar tendency was also observed for Pt(0.1) + Ni(2.6) (Fig. 3f), although the additive effect of Pt was not as significant because of the lower Pt content and higher Ni content. On the other hand, Pt(0.2)/Ni(0.9) showed a sharp peak at about 550 K (Fig. 3c); the profile of Pt(0.1)/Ni(2.6) also gave a sharp and low temperature peak (Fig. 3g). As a reference, we measured the TPR of Ni(0.9) and Ni(2.6) calcined at 573 K after reduction at 1123 K. This procedure resembled that used in the sequential impregnation method. In this procedure, nickel species were reduced to form Ni metal particles. Then, during calcination at 573 K, Ni metal particles were oxidized to NiO. Figs. 3d and 3h show a strong peak at 610 K, which can be assigned to the reduction of NiO interacted weakly with Al_2O_3 [44,45]. Compared with these Ni catalysts, the addition of Pt decreased the reduction temperature in both Pt(0.2)/Ni(0.9) and Pt(0.1)/Ni(2.6). This reduction temperature decrease is strongly

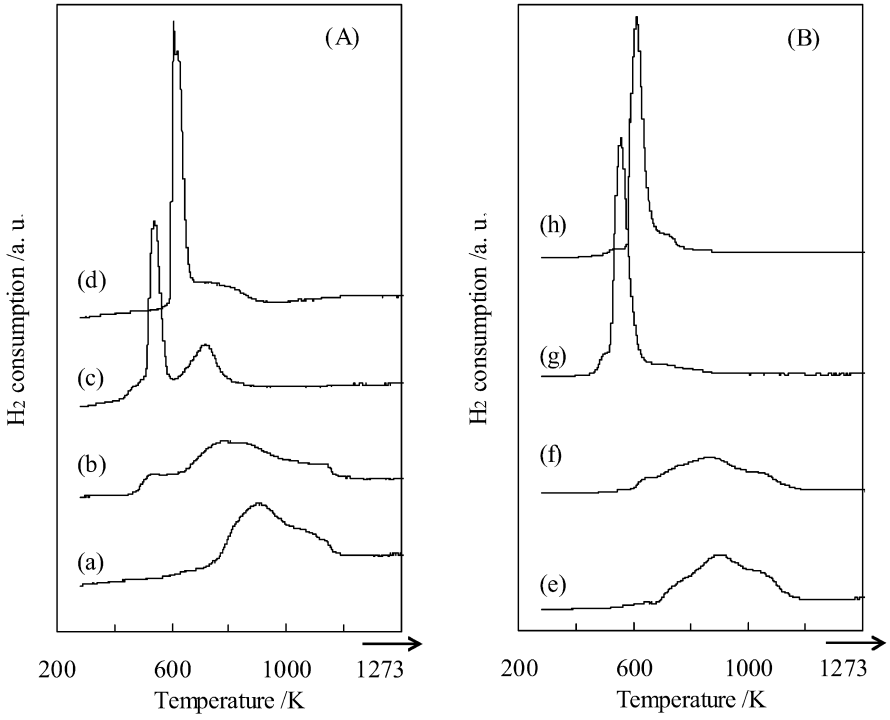

Fig. 3. Temperature-programmed reduction profiles for fresh catalysts. (A) (a) Ni(0.9), (b) Pt(0.2) + Ni(0.9), (c) Pt(0.2)/Ni(0.9) and (d) Ni(0.9)-calcined at 573 K again after reduction at 1123 K. (B) (e) Ni(2.6), (f) Pt(0.1) + Ni(2.6), (g) Pt(0.1)/Ni(2.6) and (h) Ni(2.6)-calcined at 573 K again after reduction at 1123 K. TPR conditions: 5% H_2/Ar, 10 K min^{-1}, catalyst weight 0.01 g. Intensity of H_2 consumption is normalized by the catalysts' Ni content.

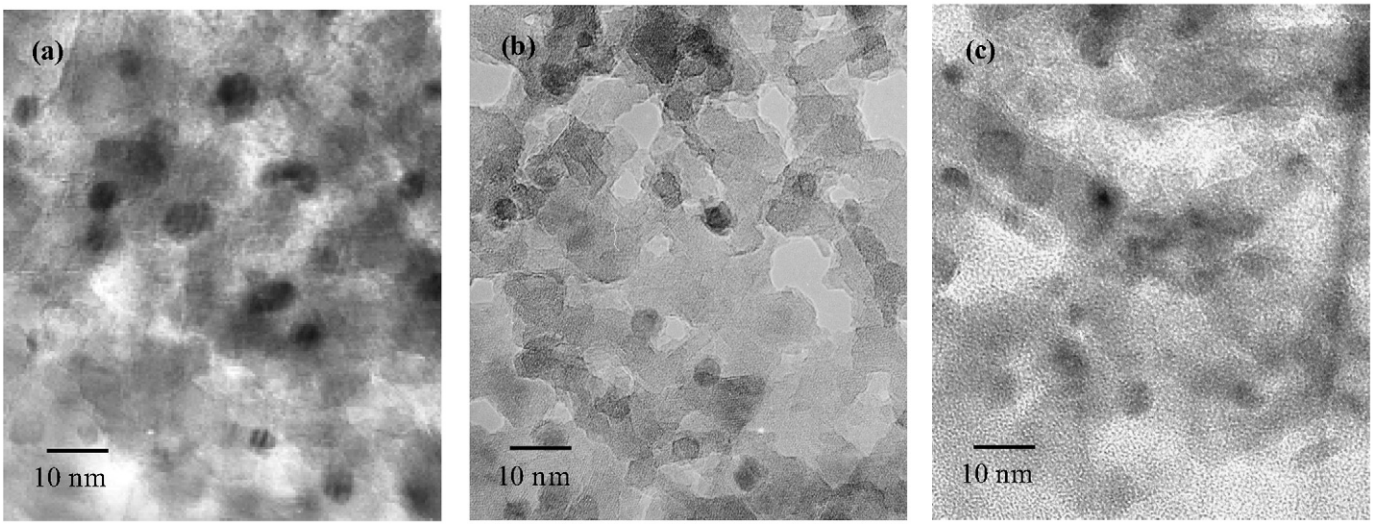

Fig. 4. TEM images of various catalysts after H_2 reduction at 1123 K for 0.5 h. (a) Ni(2.6); (b) Pt(0.1) + Ni(2.6); (c) Pt(0.1)/Ni(2.6).

Table 3
Curve fitting results of Ni K-edge EXAFS of various catalysts after reduction and passivation

Catalyst	Pretreatment[a]	Shells	CN[b]	R[c] (10^{-1} nm)	σ[d] (10^{-1} nm)	ΔE_0[e] (eV)	R_f[f] (%)
Ni(0.9)	Reduction	Ni–Ni	11.1 ± 2.5	2.49 ± 0.01	0.068 ± 0.008	−1.9 ± 3.5	0.92
	Passivation	Ni–Ni	10.5 ± 1.7	2.49 ± 0.01	0.070 ± 0.007	−2.3 ± 3.3	0.95
Pt(0.2) + Ni(0.9)	Reduction	Ni–Ni	10.2 ± 1.5	2.50 ± 0.01	0.075 ± 0.006	−0.4 ± 3.6	1.1
	Passivation	Ni–Ni	8.5 ± 1.2	2.49 ± 0.01	0.075 ± 0.005	−5.6 ± 3.2	1.2
Pt(0.2)/Ni(0.9)	Reduction	Ni–Ni	10.3 ± 1.5	2.50 ± 0.01	0.076 ± 0.006	−0.5 ± 3.1	0.83
	Passivation	Ni–Ni	10.3 ± 2.8	2.50 ± 0.01	0.074 ± 0.009	−7.3 ± 2.0	0.49
Ni foil		Ni–Ni	12	2.49	0.060	0	

[a] Sample pretreatment: reduction (H_2, 1123 K, 0.5 h), passivation (0.5% O_2, 298 K, 1 h) after the reduction.
[b] Coordination number.
[c] Bond distance.
[d] Debye–Waller factor.
[e] Difference in the origin of photoelectron energy between the reference and the sample.
[f] Residual factor. Fourier filtering range: 0.150–0.288 nm.

related to the increased catalyst reducibility achieved through the addition of Pt in the sequential impregnation method.

Fig. 4 shows TEM images of Ni(2.6), Pt(0.1) + Ni(2.6), and Pt(0.1)/Ni(2.6) catalysts after reduction. Based on the TEM images, the average particle size of metallic particles is calculated using the following equation:

$$d = \sum_i n_i d_i^3 / \sum_i n_i d_i^2,$$

where n_i is the particle number and d_i is the characteristic diameter of particles [46]. The average particles on Ni(2.6), Pt(0.1) + Ni(2.6), and Pt(0.1)/Ni(2.6) were estimated respectively as 4.8 ± 0.4, 4.5 ± 0.4, and 5.0 ± 0.4 nm. The results indicate that the metallic particles of the three catalysts are almost identical. Therefore, the catalytic performance and the bed temperature profile in oxidative steam reforming of methane cannot be interpreted by differences of the metal particle sizes.

Table 3 lists the curve-fitting results of Ni K-edge EXAFS of Ni(0.9), Pt(0.2) + Ni(0.9), and Pt(0.2)/Ni(0.9) after H_2 reduction and passivation. To analyze the position of Pt atoms in the bimetallic particles, we also measured EXAFS spectra of the catalysts after passivation using 0.5% O_2 in He. For Pt(0.2) + Ni(0.9) and Pt(0.2)/Ni(0.9), the contribution of Ni–Pt was not detected in the curve-fitting analysis, which is attributable to the low molar ratio of Pt to Ni (Pt/Ni = 0.06). The coordination number (CN) of the Ni–Ni bond over Ni(0.9) and Pt(0.2) + Ni(0.9) decreased after the passivation pretreatment, which can be explained by the oxidation of Ni metal. In addition, the contribution of Ni–O was not detected on the sample after passivation. This lack of the contribution might be related to superficial oxidation, not to the deep oxidation of Ni metal particles. In contrast, the CN over Pt(0.2)/Ni(0.9) after passivation was almost equal to that after reduction, meaning that the oxygen is not accessible to Ni species over Pt(0.2)/Ni(0.9). The addition of Pt by the sequential impregnation method suppressed oxygen accessibility to Ni.

In addition, we evaluated the composition (Pt/Ni) of each metal particle. At present, it is impossible to measure the composition of each metal particle using TEM combined with energy dispersive X-ray analysis. Therefore, we discuss the composition based only on the EXAFS results, because it can give

us the information of average structure. We found that the CN of the Ni–Ni bonds on Pt(0.2)/Ni(0.9) did not change under the passivation treatment. This indicates that the oxygen cannot access the major part of Ni. This does not guarantee the homogeneity of the composition, but it can at least ensure that the Ni particles without the interaction with Pt are in the minority; most Ni metal particles interact with the introduced Pt. If Ni metal particles are separated from the Pt atoms, we can imagine that the oxidation of Ni can be obviously detected as observed on Ni(0.9).

Fig. 5 shows the Fourier transform of Pt L_3-edge EXAFS oscillations of Pt(0.2), Pt(0.2) + Ni(0.9), and Pt(0.2)/Ni(0.9) after H_2 reduction and passivation. The peak at about 0.2 nm can be assigned to the Pt–Pt bond over Pt(0.2) after reduction and passivation. Curve-fitting results of Pt L_3-edge EXAFS are listed in Table 4. The CN of the Pt–Pt bond was almost constant on the reduced and passivated Pt(0.2). In contrast, the spectra of Pt(0.2) + Ni(0.9) after reduction and passivation were fitted to the Pt–Pt and Pt–Ni bonds; the bond lengths of Pt–Pt and Pt–Ni were much shorter than that of the intermetallic compound between Pt and Ni (NiPt and Ni_3Pt) [33]. The CNs of the Pt–Pt and Pt–Ni bonds of the bulk intermetallic compound (NiPt) were 4 and 8, respectively. In addition, regarding the intermetallic compound of Ni_3Pt, the CNs of the Pt–Pt and Pt–Ni bonds were 0 and 12, respectively [33]. These findings also indicate that the intermetallic compounds (NiPt and Ni_3Pt) were not formed on the catalyst. The bond length of Pt–Ni was nearly equal to that of Ni–Ni obtained from the Ni K-edge EXAFS results. In addition, the bond length of Pt–Pt in Pt(0.2) + Ni(0.9) was shorter than that in Pt(0.2) and Pt foil. These results suggest the formation of Pt–Ni alloy phase. The Pt atoms can partially substitute Ni atoms in Ni metal phase. These structural properties are supported by the previous report on the alloy formation of Pt–Ni [34]. In addition, when Pt and Ni are well mixed in the alloy phase, the CN ratio of Pt–Pt to Pt–Ni must correspond to its composition (Pt/Ni = 0.06). However, in the present results, the CN ratio of Pt–Pt to Pt–Ni was much higher. Therefore, it is thought that Pt can be segregated in the alloy. This is also supported by the result that the sum of the CNs of the Pt–Pt and Pt–Ni bonds was calculated as 8.2 after reduction, which is smaller than the bulk CN of fcc metal (CN = 12). This smaller CN means that some Pt atoms are located on the near surface. The CNs of both Pt–Pt and Pt–Ni were decreased by

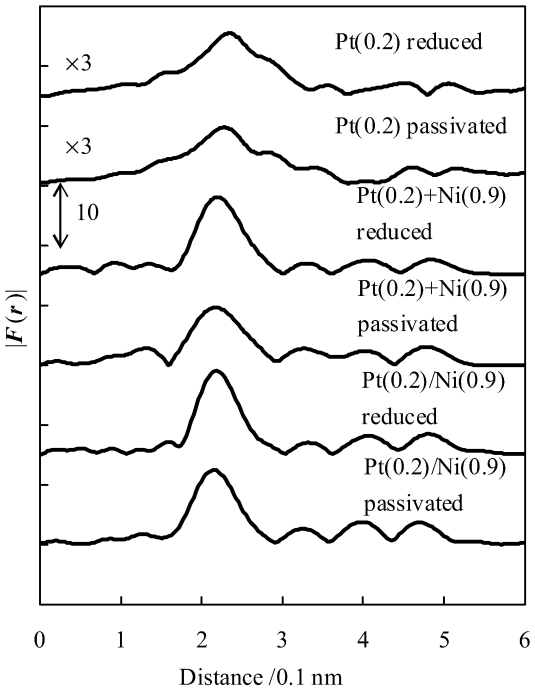

Fig. 5. Results of Fourier transform of k^3-weighted Pt L_3-edge EXAFS oscillations of Pt(0.2), Pt(0.2) + Ni(0.9) and Pt(0.2)/Ni(0.9) after the H_2 reduction and passivation. FT range: 30–129 nm^{-1}. Pretreatment: reduction (H_2, 1123 K, 0.5 h), passivation (0.5% O_2, 298 K, 1 h) after the reduction.

Table 4
Curve fitting results of Pt L_3-edge EXAFS of various catalysts after reduction and passivation

Catalyst	Pretreatment[a]	Shells	CN[b]	R[c] (10^{-1} nm)	σ[d] (10^{-1} nm)	ΔE_0[e] (eV)	R_f[f] (%)
Pt(0.2)	Reduction	Pt–Pt	10.5 ± 2.2	2.72 ± 0.02	0.112 ± 0.006	−3.2 ± 4.9	1.8
	Passivation	Pt–Pt	10.5 ± 2.3	2.71 ± 0.02	0.115 ± 0.007	−5.1 ± 5.3	2.3
Pt(0.2) + Ni(0.9)	Reduction	Pt–Pt	3.7 ± 1.1	2.65 ± 0.01	0.070 ± 0.008	−7.2 ± 4.0	0.14
		Pt–Ni	4.5 ± 0.6	2.52 ± 0.01	0.070 ± 0.003	−6.2 ± 1.4	
	Passivation	Pt–Pt	3.2 ± 1.5	2.65 ± 0.02	0.070 ± 0.013	−7.5 ± 4.5	0.48
		Pt–Ni	3.3 ± 0.5	2.51 ± 0.01	0.070 ± 0.007	−1.2 ± 2.9	
Pt(0.2)/Ni(0.9)	Reduction	Pt–Pt	2.8 ± 1.0	2.65 ± 0.02	0.070 ± 0.011	−6.5 ± 4.5	0.1
		Pt–Ni	4.3 ± 0.3	2.52 ± 0.01	0.063 ± 0.003	−6.5 ± 1.3	
	Passivation	Pt–Pt	2.7 ± 1.1	2.69 ± 0.03	0.070 ± 0.014	−2.0 ± 6.0	0.85
		Pt–Ni	4.2 ± 1.1	2.52 ± 0.02	0.070 ± 0.010	−4.7 ± 3.6	
Pt foil		Pt–Pt	12	2.77	0.060	0	

[a] Sample pretreatment: reduction (H_2, 1123 K, 0.5 h), passivation (0.5% O_2, 298 K, 1 h) after the reduction.
[b] Coordination number.
[c] Bond distance.
[d] Debye–Waller factor.
[e] Difference in the origin of photoelectron energy between the reference and the sample.
[f] Residual factor. Fourier filtering range: 0.160–0.301 nm.

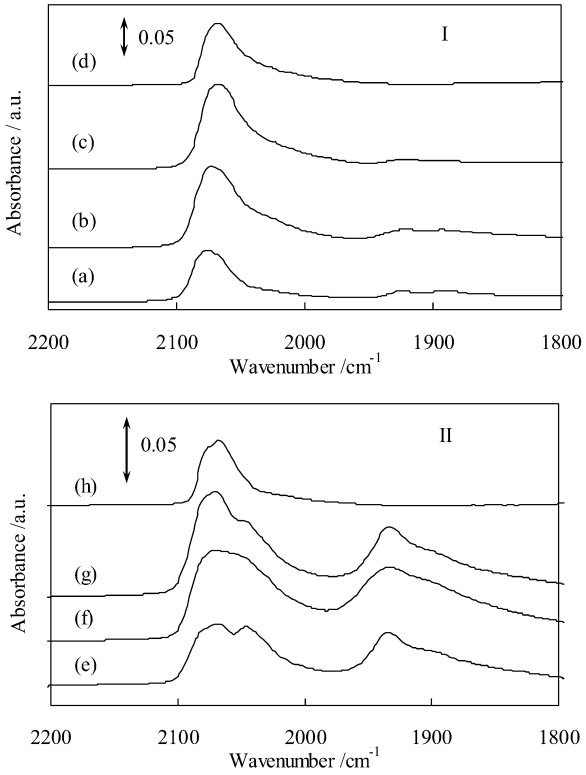

Fig. 6. FTIR spectra of CO adsorption at room temperature: (I) (a) Ni(0.9), (b) Pt(0.2) + Ni(0.9), (c) Pt(0.2)/Ni(0.9), (d) Pt(0.2); (II) (e) Ni(2.6), (f) Pt(0.1) + Ni(2.6), (g) Pt(0.1)/Ni(2.6), (h) Pt(0.1).

the passivation pretreatment, and the CN of the Pt–Ni bond decreased more significantly than that of the Pt–Pt bond in Pt(0.2) + Ni(0.9), which can be attributed to higher accessibility of oxygen to Ni. Furthermore, the spectra of Pt(0.2)/Ni(0.9) after the reduction and passivation were also fitted by the Pt–Pt and Pt–Ni bonds, and the results regarding the bond length were similar to those of Pt(0.2) + Ni(0.9). The sum of CNs of the Pt–Pt and Pt–Ni bonds on Pt(0.2)/Ni(0.9) was estimated as 7.1, smaller than that of Pt(0.2) + Ni(0.9), suggesting that the ratio of surface Pt atoms on Pt(0.2)/Ni(0.9) was much higher than that on Pt(0.2) + Ni(0.9). In addition, the contribution of Pt–Ni to the CN was larger than that of Pt–Pt in Pt(0.2)/Ni(0.9). It is presumed that greater Pt–Ni interaction resulted from the sequential impregnation method than from the co-impregnation method. From the results, we can also infer that the structure of Pt(0.2)/Ni(0.9) has higher resistance to oxidation than that of Pt(0.2) + Ni(0.9), as revealed by Pt L_3-edge EXAFS analysis.

The FTIR spectra of CO adsorption were measured to characterize surface properties of Pt–Ni bimetallic particles. Fig. 6I shows that the spectra of four catalysts were very similar. With the Ni (0.9) catalyst (Fig. 6a), the band at 2080 cm^{-1} can be attributed to linear CO on Ni [47,48]. In addition, a very small band assigned to bridge CO was observed at 1930 cm^{-1} [49]. For the monometallic Pt catalyst (Fig. 6d), only one band was observed at 2070 cm^{-1}, which is assigned to linear CO [50–52]. In the cases of Pt(0.2) + Ni(0.9) and Pt(0.2)/Ni(0.9) (Fig. 6, curves b and c), the band at 2070 cm^{-1} was observed, similar to those of the Ni(2.6) and Pt(0.2) catalysts. It is difficult to detect structural differences between Pt(0.2) + Ni(0.9) and Pt(0.2)/Ni(0.9) because of the similarity of linear CO on Ni and on Pt. In contrast, structures differed greatly for catalysts with higher Ni loadings. For the Ni(2.6) catalyst (Fig. 6e), the bands at 2070 and 2050 cm^{-1} are attributable to the linear CO on Ni metal; the band at about 1930 cm^{-1} is assigned to the bridge CO. Compared with the spectrum of Ni(0.9), the relative intensity of bridge CO increased significantly over that of Ni(2.6). For the monometallic Pt catalyst (Fig. 6h), only one band was observed at 2070 cm^{-1}, which was assigned to linear CO. In the case of Pt(0.1) + Ni(2.6) (Fig. 6f), two broad bands at 2070 and 2048 cm^{-1} with similar intensity were observed; these bands were similar to those of the Ni(2.6) catalyst. In contrast, for Pt(0.1)/Ni(2.6) (Fig. 6g), the intensity of the band at 2070 cm^{-1} was much stronger than that of the band at 2048 cm^{-1}. The difference of spectra between Pt(0.1)/Ni(2.6) and Ni(2.6) was caused by the peak intensity at 2070 cm^{-1}, which is due to linear CO on Pt. Judging from the FTIR of CO adsorption, the Pt atoms were located on the surface of metal particles more preferentially on the catalyst prepared using the sequential impregnation method. This tendency is also supported by the EXAFS results. The salient implication of this finding is that the sequential impregnation method is more effective than the co-impregnation method in terms of surface modification, particularly with a small amount of Pt. The combination of EXAFS and FTIR results suggests segregation of Pt atoms on the surface of the Pt–Ni alloy particles.

In the oxidative steam reforming of methane, the oxidation state on Ni can depend strongly on the position in the catalyst bed, because the partial pressure of introduced oxygen is rather high at the catalyst bed inlet, but it is almost zero at the bed outlet because O_2 conversion was almost 100% in all of these experimental conditions at $T_{TC} = 1123$ K. The TPR profile of the catalyst near the inlet and outlet were obtained to elucidate the dependence of the catalyst oxidation state on the position in the catalyst bed. In this experiment, the catalyst was purged with Ar after the reaction treatment ($CH_4/H_2O/O_2/Ar = 40/30/20/10$, $W/F = 0.16$ g h mol^{-1}, 1123 K, $W = 0.08$ g), then cooled rapidly from the reaction temperature (1123 K) to room temperature. Then the catalysts at the bed inlet and outlet were carefully divided; the amount of the divided catalysts was 0.01 g. Judging from the thermographic results, the size of the exothermic zone was as large as a quarter of the catalyst bed, where the total amount of the catalyst was 0.08 g. Therefore, the amount of the divided catalyst was suitable for the analysis of the catalyst bed inlet and outlet. Fig. 7A shows TPR profiles of fresh and used Ni(2.6) catalyst. Ni(2.6) was reduced completely at 700–1000 K (Fig. 7A, a), as discussed above. This is assigned to NiO interacting strongly with the Al_2O_3 surface [41]. On the other hand, two TPR peaks were observed for the catalyst at the bed inlet after the reaction (Fig. 7A, b). The lower temperature peak (650–760 K) can be assigned to NiO, which interacted weakly with the Al_2O_3 surface [44,45], as shown in Fig. 3. The higher temperature peak at 1150 K is attributed to the reduction of $NiAl_2O_4$ compound [53–55], which can be formed by a solid-state reaction between NiO and Al_2O_3. The H_2 consumption for the reduction of the NiO and $NiAl_2O_4$ were 70

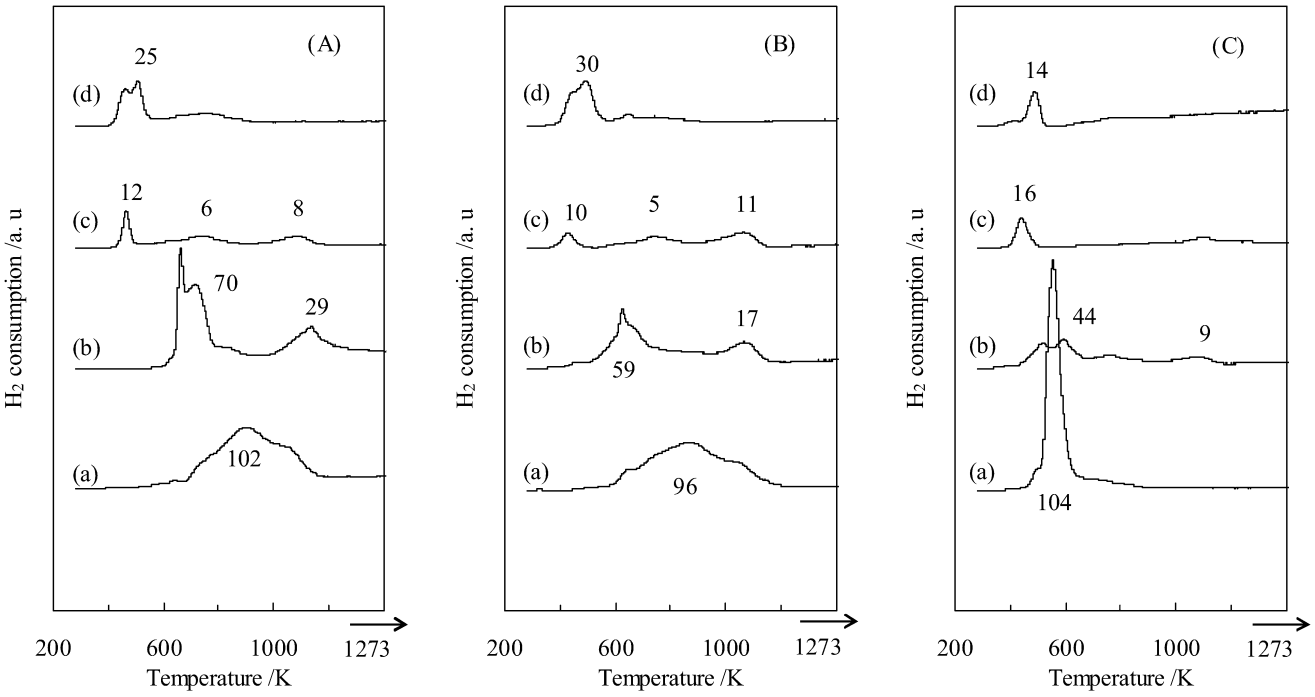

Fig. 7. Temperature-programmed reduction profiles for (A) Ni(2.6), (B) Pt(0.1) + Ni(2.6) and (C) Pt(0.1)/Ni(2.6) catalysts: (a) fresh catalysts before H_2 reduction pretreatment; (b) the catalyst at bed inlet after $CH_4/H_2O/O_2/Ar = 40/30/20/10$; (c) the catalyst at bed outlet after $CH_4/H_2O/O_2/Ar = 40/30/20/10$; (d) fresh catalyst after reduction at 1123 K, 0.5 h. The value near each peak is the ratio of H_2 consumption on the basis of $H_2/Ni = 100\%$.

and 29%, respectively, indicating that most Ni species at the catalyst bed inlet were oxidized during the reaction. In contrast, a peak at 470 K was observed for the catalyst at the bed outlet (Fig. 7A, c), which resembles that of the reduced sample (Fig. 7A, d). This resemblance indicates that the metallic Ni species were present on the catalyst at the outlet under the reaction condition, which is ascribed mainly to the absence of oxygen in the gas phase at the catalyst bed outlet. It is noteworthy that a small amount of H_2 consumption was observed in the TPR profile of the reduced sample (Fig. 7A, d), which is attributable to the reduction of adsorbed oxygen on the Ni metal surface. This oxygen is adsorbed during the transfer of the sample in the air from the reactor to the TPR cell. Except at the inlet part (Fig. 7B, b), under the reaction condition, Pt(0.1) + Ni(2.6) (Fig. 7B) displayed a similar TPR behavior to that of Ni(2.6). The amount of H_2 consumption in the lower temperature peak was decreased to 59% on Pt(0.1) + Ni(2.6) at the bed inlet. In addition, the maximum reduction of Ni oxide was observed at 630 K, which is about 40 K lower than the reduction of Ni in Ni(2.6) (Fig. 7A, b). Fig. 7C shows TPR results for the Pt(0.1)/Ni(2.6) catalyst. An important point to note is that at the catalyst bed inlet, the reduction peak shifted to a much lower temperature region, around 530–610 K, corresponding to 44% of the total Ni amount. These results indicate that the addition of Pt by the sequential impregnation method greatly increased the amount of reduced Ni at the catalyst bed inlet, even under the presence of O_2 in the gas phase during oxidative steam reforming of methane. TPR profiles demonstrate that the reducibility on Pt–Ni bimetallic catalysts and resistance to Ni oxidation were strongly influenced by the preparation method; this result is in agreement with the suggestion by EXAFS and FTIR findings that the Pt atoms introduced by the sequential impregnation method were located more preferentially on the surface of Pt–Ni bimetallic particles.

The effect of Pt addition on the resistance to the oxidation of Ni is thought to be either a thermodynamic or kinetic effect. We believe that the additive effect is mainly a kinetic effect, because the oxidized Ni species can be reduced to some extent by the reactant gas of oxidative steam reforming of methane, as demonstrated in the increasing temperature profile in Fig. 1a. Therefore, the ratio of reduced to oxidized Ni species can be strongly dependent on the reduction rate of oxidized species and the oxidation rate of reduced species. As described above, the shift of H_2 consumption peak to the lower temperature in TPR profiles (Fig. 7) indicates that Pt modification enhances the reduction rate of Ni species. At the same time, the much lower sticking probability of O_2 on the Pt surface [56,57] than that on the Ni surface [58,59] leads us to consider that the oxidation rate of Ni^0 can be decreased on the Pt-modified Ni surface. This can be demonstrated by the enhanced reduction rate of the oxidized Ni species and the decreased oxidation rate of Ni^0 species by the surface modification of Ni with Pt. This indicates that the addition of Pt enhances the resistance to oxidation of Ni, and also that the addition of Pt is more effective in the sequential impregnation method than in the co-impregnation method, due to the difference in the segregation of Pt–Ni surface alloy.

The relationship between the catalytic performance (including the bed temperature profile) and the surface modification of Ni particles with Pt has been evaluated. A large temperature gradient over Ni catalysts in oxidative steam reforming of methane has been reported previously [6,13,15–17,25,60]. As shown in Fig. 7, most Ni species were oxidized in the pres-

ence of oxygen (e.g., at the catalyst bed inlet). This is because the rate of Ni oxidation by O_2 is much higher than the reduction of oxidized Ni species with reducing agents like CH_4, CO, and H_2, as demonstrated by the hysteresis shown in Fig. 1. As a result, the oxidized Ni species loses reforming activity and has only combustion activity. Therefore, at the catalyst bed inlet, only the exothermic reaction can proceed, which increases the catalyst bed temperature. In contrast, in the region with no oxygen (e.g., at the catalyst bed outlet), the Ni species can be maintained in the metallic state and presents the reforming activity. In this reaction zone, only the endothermic reaction can proceed, and the catalyst bed temperature decreases. This can result in a large temperature gradient. In contrast, on the Pt/Ni catalysts, the ratio of reduced species to oxidized species can be much higher, due to the modification effect of Pt in the presence of oxygen. In particular, the reduced species can also be the active site for methane reforming as well as combustion even in the presence of oxygen, and the reforming reaction can contribute to the decreased temperature at the catalyst bed inlet.

4. Conclusion

Monometallic Ni catalyst showed hysteresis with respect to temperature increases and decreases in the oxidative steam reforming of methane ($CH_4/H_2O/O_2/Ar = 40/30/20/10$). This behavior can be explained by the oxidation of Ni metal species with O_2 due to the higher oxidation rate of the metallic species compared with the reduction rate of the oxidized species. Although the monometallic Ni catalysts exhibited high catalytic activity in the steam reforming of methane without the addition of oxygen ($CH_4/H_2O/O_2/Ar = 30/30/0/40$), in the oxidative steam reforming of methane at 1123 K, the Ni species near the bed inlet were oxidized in the presence of oxygen, which greatly decreased the performance. Oxidized Ni does not have the reforming activity, and the combustion reaction proceeds at the catalyst bed inlet, resulting in a high bed temperature and a large temperature gradient.

The hysteresis with respect to temperature increases and decreases in the oxidative steam reforming of methane over the monometallic Ni catalysts disappeared with the modification of the catalysts with Pt. The additive effect of Pt by the sequential impregnation method (Pt/Ni) was much more significant than that by the co-impregnation method (Pt + Ni). This is due to the tendency of the Pt atoms on the Pt/Ni catalysts to be located more preferably on the surface to form Pt–Ni alloy compared with those on the Pt + Ni, as supported by the characterization results. The superior performance of the catalyst prepared by the sequential impregnation method (Pt/Ni) can be attributed mainly to the effective inhibition of Ni oxidation near the bed inlet in the oxidative steam reforming of methane at 1123 K. This can be due to the decrease in oxidation rate and increase in reduction rate caused by surface modification of Ni with Pt. The Pt–Ni species are maintained in the metallic state near the bed inlet, which can be the active site for the reforming reaction as well as the combustion reaction, and this can be related to lower bed temperature and smaller temperature gradient than for the monometallic Ni catalysts.

Acknowledgments

This study was supported by the Industrial Technology Research Grant Program (05A43002C) of the New Energy and Industrial Technology Development Organization of Japan. The EXAFS studies were performed under the approval of the Photon Factor Advisory Committee (Proposal 2006G095).

References

[1] J.R. Rostrup-Nielsen, J. Sehested, J.K. Norskov, Adv. Catal. 47 (2002) 65.
[2] J.R. Rostrup-Nielsen, Catalysis: Science and Technology, vol. 5, Springer-Verlag, New York, 1984.
[3] K. Aasberg-Petersen, J.-H. Bak Hansen, T.S. Christensen, I. Dybkjaer, P. Seier Christensen, C. Stub Nielsen, S.E.L. Winter Madsen, J.R. Rostrup-Nielsen, Appl. Catal. A 221 (2001) 379.
[4] M.C.J. Bradford, M.A. Vannice, Catal. Rev. Sci. Eng. 41 (1999) 1.
[5] J.R. Rostrup-Nielsen, Catal. Today 71 (2002) 243.
[6] J.R. Rostrup-Nielsen, J.H.B. Hansen, L.M. Aparicio, Sekiyu Gakkaishi 40 (1997) 366.
[7] A.M. O'Connor, J.R.H. Ross, Catal. Today 46 (1998) 203.
[8] D. Dissanayake, M.P. Rosynek, J.H. Lunsford, J. Phys. Chem. 97 (1993) 3644.
[9] D. Dissanayake, M.P. Rosynek, K.C.C. Kharas, J.H. Lunsford, J. Catal. 132 (1991) 117.
[10] B. Li, K. Maruyama, M. Nurunnabi, K. Kunimori, K. Tomishige, Ind. Eng. Chem. Res. 44 (2005) 485.
[11] K. Tomishige, Y. Matsuo, M. Asadullah, Y. Yoshinaga, Y. Sekine, K. Fujimoto, ACS Symp. Ser. 809 (2002) 303.
[12] K. Tomishige, S. Kanazawa, M. Sato, K. Ikushima, K. Kunimori, Catal. Lett. 84 (2002) 69.
[13] K. Tomishige, M. Nurunnabi, K. Maruyama, K. Kunimori, Fuel Process. Technol. 85 (2004) 1103.
[14] K. Tomishige, S. Kanazawa, S. Ito, K. Kunimori, Appl. Catal. A 244 (2003) 71.
[15] A.M. O'Connor, J.R.H. Ross, Catal. Today 46 (1998) 203.
[16] Y.H. Hu, E. Ruckenstein, Adv. Catal. 48 (2004) 297.
[17] A.M. De Groote, G.F. Froment, Appl. Catal. A Gen. 138 (1996) 245.
[18] F. Basile, G. Fornasari, F. Trifiro, A. Vaccari, Catal. Today 64 (2001) 21.
[19] K. Takehira, T. Shishido, P. Wang, T. Kosaka, K. Takaki, J. Catal. 221 (2004) 43.
[20] V.R. Choudhary, K.C. Mondal, A.S. Mamman, J. Catal. 233 (2005) 36.
[21] K. Nagaoka, A. Jentys, J.A. Lercher, J. Catal. 229 (2005) 185.
[22] V.R. Choudhary, K.C. Mondal, T.V. Choudhary, Appl. Catal. A 306 (2006) 45.
[23] V.R. Choudhary, K.C. Mondal, T.V. Choudhary, Chem. Eng. J. 121 (2006) 73.
[24] M. Nurunnabi, K. Fujimoto, K. Suzuki, B.T. Li, S. Kado, K. Kunimori, K. Tomishige, Catal. Commun. 7 (2006) 73.
[25] K. Tomishige, S. Kanazawa, K. Suzuki, M. Asadullah, M. Sato, K. Ikushima, K. Kunimori, Appl. Catal. A 233 (2002) 35.
[26] B. Li, K. Maruyama, M. Nurunnabi, K. Kunimori, K. Tomishige, Appl. Catal. A 275 (2004) 71.
[27] T.B. Reed, Free Energy Formation of Binary Compounds, MIT Press, Cambridge, 1971.
[28] B.T. Li, S. Kado, Y. Mukainakano, M. Nurunnabi, T. Miyao, S. Naito, K. Kunimori, K. Tomishige, Appl. Catal. A 304 (2006) 62.
[29] S. A Lee, K.W. Park, J.H. Choi, B.K. Kwon, Y.E. Sung, J. Electrochem. Soc. 149 (2002) A1299.
[30] T.C. Deivaraj, J.Y. Lee, J. Electrochem. Soc. 151 (2004) A1832.
[31] T.C. Deivaraj, W.X. Chen, J.Y. Lee, J. Mater. Chem. 13 (2003) 2555.
[32] J.C. Bertolini, Surf. Rev. Lett. 3 (1996) 1857.
[33] A. Jentys, G.L. Haller, J.A. Lercher, J. Phys. Chem. 97 (1993) 484.
[34] A.S. Bommannavar, P.A. Montano, M.J. Yacamn, Surf. Sci. 156 (1985) 426.
[35] J.W. Cook, D.E. Sayers, J. Appl. Phys. 52 (1981) 5024.

[36] K. Okumura, J. Amano, N. Yasunobu, M. Niwa, J. Phys. Chem. B 104 (2000) 1050.
[37] K. Okumura, S. Matsumoto, N. Nishiaki, M. Niwa, Appl. Catal. B Environ. 40 (2003) 151.
[38] A.L. Ankudinov, B. Ravel, J.J. Rehr, S.D. Conradson, Phys. Rev. B 58 (1998) 7565.
[39] O. Yamazaki, K. Tomishige, K. Fujimoto, Appl. Catal. A 136 (1996) 49.
[40] M. Nurunnabi, B. Li, K. Kunimori, K. Suzuki, K.-I. Fujimoto, K. Tomishige, Appl. Catal. A 292 (2005) 272.
[41] J. Wang, L. Dong, Y.-H. Hu, G.-S. Zheng, Z. Hu, Y. Chen, J. Solid State Chem. 157 (2001) 274.
[42] M. Nurunnabi, B. Li, K. Kunimori, K. Suzuki, K.-I. Fujimoto, K. Tomishige, Catal. Lett. 103 (2005) 277.
[43] Y.-G. Chen, O. Yamazaki, K. Tomishige, K. Fujimoto, Catal. Lett. 39 (1999) 91.
[44] Y.-J. Chu, Z.-B. Wei, S.-W. Yang, C. Li, Q. Xin, E.-Z. Min, Appl. Catal. A 176 (1999) 17.
[45] S.-B. Wang, G.-Q. Lu, Appl. Catal. A 169 (1998) 271.
[46] D.G. Mustard, C.H. Bartholomew, J. Catal. 67 (1981) 186.
[47] G. Poncelet, M.A. Centeno, R. Molina, Appl. Catal. A 288 (2005) 232.
[48] C. Hu, Y. Chen, P. Li, H. Min, Y. Chen, A. Tian, J. Mol. Catal. A 110 (1996) 163.
[49] T. Ueckert, R. Lamber, N.I. Jaeger, U. Schubert, Appl. Catal. A 155 (1997) 75.
[50] X. Li, X. You, P. Ying, J. Xiao, C. Li, Top. Catal. 25 (2003) 63.
[51] E.L. Jablonski, A.A. Castro, O.A. Scelza, S.R. de Miguel, Appl. Catal. A 183 (1999) 189.
[52] D. Liu, G.-H. Que, Z.-X. Wang, Z.-F. Yan, Catal. Today 68 (2001) 155.
[53] B.T. Li, R. Watanabe, K. Maruyama, M. Nurunnabi, K. Kunimori, K. Tomishige, Appl. Catal. A 290 (2005) 36.
[54] A. Gil, A. Diaz, L.M. Gandia, M. Montes, Appl. Catal. A 109 (1994) 167.
[55] J.M. Rynkowski, T. Paryjczak, M. Lenik, Appl. Catal. A 106 (1993) 73.
[56] C.T. Campbell, G. Ertl, H. Kuipers, J. Segner, Surf. Sci. 107 (1981) 220.
[57] A.C. Luntz, M.D. Williams, D.S. Bethune, J. Chem. Phys. 89 (1988) 4381.
[58] J.T. Stuckless, C.E. Wartnaby, N. Al-Sarraf, St.J.B. Dixon-Warren, M. Kovar, D.A. King, J. Chem. Phys. 106 (1997) 2012.
[59] K. Yagi-Watanabe, Y. Ikeda, Y. Ishii, T. Inokuchi, H. Fukutani, Surf. Sci. 482–485 (2001) 128.
[60] B.T. Li, R. Watanabe, K. Maruyama, M. Nurunnabi, K. Kunimori, K. Tomishige, Catal. Today 104 (2005) 7.